

Research Article

Open Access



# Integrating Cu/Cu<sub>x</sub>O ternary nanocomposites with multi-walled carbon nanotubes enabling a high-performance nonenzymatic amperometric glucose sensor

Weiyan Xi<sup>1</sup>, Yupeng Zhang<sup>1</sup>, Zhijia Zhang<sup>1</sup>, Yu Chen<sup>1</sup>, Xuanyuan Huang<sup>2</sup>, Hongwei Mou<sup>2</sup>, Zhaoxue Deng<sup>3</sup>, Zhen Li<sup>1</sup>, Xiaoxue Xu<sup>2</sup>, Wei Zheng<sup>1</sup>

<sup>1</sup>Institute of Surface/Interface Science and Technology, Key Laboratory of Superlight Material and Surface Technology of Ministry of Education, College of Materials Science and Chemical Engineering, Harbin Engineering University, Harbin 150001, Heilongjiang, China.

<sup>2</sup>School of Biomedical Engineering, Faculty of Engineering and Information Technology, University of Technology Sydney, Ultimo, NSW 2007, Australia.

<sup>3</sup>School of Architecture and Civil Engineering, Harbin University of Science and Technology, Harbin 150001, Heilongjiang, China.

**Correspondence to:** Prof. Wei Zheng, Institute of Surface/Interface Science and Technology, Key Laboratory of Superlight Material and Surface Technology of Ministry of Education, College of Materials Science and Chemical Engineering, Harbin Engineering University, 145 Nantong St., Harbin 150001, Heilongjiang, China. E-mail: zhengwei@hrbeu.edu.cn; Dr. Xiaoxue Xu, School of Biomedical Engineering, Faculty of Engineering and Information Technology, University of Technology Sydney, 15 Broadway, Ultimo, NSW 2007, Australia. E-mail: xiaoxuehelen.xu@uts.edu.au; Prof. Zhen Li, Institute of Surface/Interface Science and Technology, Key Laboratory of Superlight Material and Surface Technology of Ministry of Education, College of Materials Science and Chemical Engineering, Harbin Engineering University, 145 Nantong St., Harbin 150001, Heilongjiang, China. E-mail: lz\_heu@163.com

**How to cite this article:** Xi W, Zhang Y, Zhang Z, Chen Y, Huang X, Mou H, Deng Z, Li Z, Xu X, Zheng W. Integrating Cu/Cu<sub>x</sub>O ternary nanocomposites with multi-walled carbon nanotubes enabling a high-performance nonenzymatic amperometric glucose sensor. *Microstructures* 2024;4:2024028. <https://dx.doi.org/10.20517/microstructures.2023.79>

**Received:** 30 Nov 2023 **First Decision:** 8 Feb 2024 **Revised:** 9 Mar 2024 **Accepted:** 1 Apr 2024 **Published:** 16 May 2024

**Academic Editor:** Sophia Gu **Copy Editor:** Fangling Lan **Production Editor:** Fangling Lan

## Abstract

We developed a new nonenzymatic amperometric glucose sensor by integrating a ternary nanocomposite, Cu/Cu<sub>2</sub>O/CuO (Cu/Cu<sub>x</sub>O), with multi-wall carbon nanotubes (Cu/Cu<sub>x</sub>O@MWCNTs) as the electrocatalyst. The Cu/Cu<sub>x</sub>O@MWCNTs nanocomposite is prepared via an electroless plating process followed by thermal treatment. The constructed nanocomposites are systematically characterized with a transmission electron microscope, an X-ray diffractometer, Fourier transform infrared spectroscopy, X-ray photoelectron spectroscopy, and electrochemical impedance spectroscopy, respectively. The Cu/Cu<sub>x</sub>O@MWCNTs nanocomposites-modified



© The Author(s) 2024. **Open Access** This article is licensed under a Creative Commons Attribution 4.0 International License (<https://creativecommons.org/licenses/by/4.0/>), which permits unrestricted use, sharing, adaptation, distribution and reproduction in any medium or format, for any purpose, even commercially, as long as you give appropriate credit to the original author(s) and the source, provide a link to the Creative Commons license, and indicate if changes were made.



glassy carbon electrodes exhibit high electrocatalytic activity toward glucose electrooxidation under alkaline conditions. The efficient electrocatalytic activity of Cu/Cu<sub>x</sub>O@MWCNTs for glucose electrooxidation is utilized for glucose detection using Cu/Cu<sub>x</sub>O@MWCNTs-modified glassy carbon electrodes. The Cu/Cu<sub>x</sub>O@MWCNTs-modified electrode displays an excellent sensing performance within a wide analyte concentration from 0.005-6,000 M (low detection limit is calculated to be 0.003 μM) with superior stability, selectivity, repeatability, and reproductivity. This as-prepared electrochemical sensor is successfully applied to selective glucose detection with satisfactory results.

**Keywords:** Electrocatalyst, Cu/Cu<sub>x</sub>O ternary nanocomposites, electrochemical, nonenzymatic sensor, amperometric detection

## INTRODUCTION

Diabetes is a metabolic disorder syndrome featuring high blood glucose levels<sup>[1]</sup>, making it one of the three biggest killers of human health worldwide, following cardiovascular disease and cancer. It is projected to affect 693 million people (aged 18-99) by 2045, a 54% increase compared to 2017<sup>[2]</sup>. As a result, developing rapid, accurate and convenient methods for detecting glucose levels<sup>[3,4]</sup> in human blood or serum is crucial for diagnosing and managing diabetes within clinical practice. In 1962, Clark and Updike elaborated the first enzyme electrodes and current-based enzyme sensors<sup>[5-7]</sup>. Even though as many as 85% of commercial glucose sensors are enzyme-based electrochemical biosensors<sup>[8]</sup>, there has been an instability of this type of enzyme-based biosensors<sup>[9-11]</sup>. This instability is primarily due to the sensitivity of glucose oxidase to environmental conditions (e.g., temperature<sup>[12]</sup>, humidity<sup>[13]</sup>, and pH<sup>[14]</sup>). It is challenging to establish a reliable method toward glucose by enzyme-based electrochemical biosensors.

Additionally, the applications of enzyme-based biosensors are largely restricted due to issues such as complicated immobilization processes, sophisticated operating conditions, poor reproducibility, and prohibitive costs<sup>[3,15-17]</sup>. To surmount the aforementioned weaknesses, scholars proposed a nonenzymatic sensor based on the direct electrochemical reaction toward glucose, which has been rapidly developed. Previous studies have shown that this nonenzymatic sensor relies on the electrical signal produced during the glucose oxidation on the surface of the electrode. The electrocatalytic activity of electrode materials is the key aspect influencing glucose sensing sensitivity and selectivity<sup>[8]</sup>.

To date, noble metals and their oxides (e.g., Pt<sup>[18]</sup>, Pd<sup>[19]</sup>, Au, Ag, and various alloy particles<sup>[20,21]</sup>) have been utilized in the construction of nonenzymatic biosensors for detecting glucose. While they possess superior electrocatalytic properties for glucose oxidation, they are susceptible to contamination through chemisorption of intermediates or chloride adsorption<sup>[22]</sup>. The stability and sensitivity of the sensors are reduced when they are modified with noble metals or their oxides, limiting their widespread use in glucose detection. Transition metals and their oxides, such as Ni<sup>[23]</sup>, Cu<sup>[21]</sup>, MnO<sub>2</sub><sup>[24]</sup>, CuO<sup>[25]</sup>, Cu<sub>2</sub>O<sup>[26]</sup>, Co<sub>3</sub>O<sub>4</sub><sup>[27]</sup>, and ZnO<sup>[28]</sup>, have demonstrated increasing application potential on account of resourceful, biocompatible, relatively inexpensive, and excellent glucose sensing capability. Among these, copper and its oxides exhibit attractive application prospects due to their low cost and outstanding catalytic performance for various reactions. For quite some time, they have been capable of catalyzing the electrochemical oxidation of glucose. For example, Cu<sup>[21]</sup>, Cu<sub>2</sub>O<sup>[26]</sup>, CuO<sup>[25]</sup>, and Cu<sub>2</sub>S<sup>[29]</sup> have been applied for the direct modification of nonenzymatic glucose biosensors.

Furthermore, alloys, nanocomposite materials consisting of bimetallic alloy and their oxides, metal/metal oxide, and 1D or 2D carbon nanomaterials tend to manifest synergistic effects from the constituent

metals<sup>[30]</sup>. The large surface area of nanocomposite facilitates the exposure of numerous electrochemically active sites for the glucose reactions<sup>[31]</sup>. Fan *et al.* demonstrated that a bimetallic alloy nanoparticles-modified 3D graphene nanocomplex, Au-Ag/3D graphene, exhibited excellent electrocatalytic properties towards glucose<sup>[32]</sup>. Studies on the nanocomposite of copper oxide anchored polyaniline to modify the electrode by Sudharsan *et al.* have shown superior electrochemical determination of chlorpyrifos<sup>[33]</sup>. In contrast, multi-walled carbon nanotubes (MWCNTs) are gaining recognition as promising electrode materials due to their hollow tubular nanostructure, high surface area, remarkable electrical conductivity, exceptional stability, and promising potential for glucose detection<sup>[34]</sup>. To enhance the electrical conductivity of copper oxides and improve the stability and dispersion of copper and its oxides, researchers have deposited them on various substrates<sup>[21,26]</sup> using MWCNTs as a representative example. Most studies have focused on two-phase composites of metals and their oxides<sup>[20]</sup>. Building on the above research, integrating triple materials could be a compelling option for nonenzymatic glucose detection. The different properties of the various materials and sufficient exposure of active metal species on MWCNT surfaces will have multiple promotions on electrochemical activity.

Herein, Cu/Cu<sub>x</sub>O ternary nanocomposites have been successfully modified onto the surface of MWCNTs by the electroless plating and further heat treatment to obtain Cu/Cu<sub>x</sub>O@MWCNTs nanocomposites. These acquired nanocomposites demonstrate superior nonenzymatic electrocatalytic activity towards glucose. By taking advantage of their high-performance catalytic activity for glucose oxidation, we developed an electrochemical biosensor for glucose based on Cu/Cu<sub>x</sub>O@MWCNTs nanocomposites-modified electrodes and investigated their electrocatalytic application. A schematic diagram illustrating the electrochemical sensing using Cu/Cu<sub>x</sub>O@MWCNTs ternary nanocomposites-based sensors is presented in [Scheme 1](#).

## MATERIALS AND METHODS

### Chemicals and materials

CuSO<sub>4</sub>·5H<sub>2</sub>O was acquired from Yaohua Chemical Reagent Co., Ltd., Tianjin, China. NaOH was gained from the Mainland Chemical Reagent Factory (Tianjin, China). Glucose was obtained from Ruijinte Chemical Co., Ltd. (Tianjin, China). The serum of healthy volunteers was sourced from a hospital in Nanjing. All aqueous solutions were prepared and diluted with deionized water from Hitech-Kflow (Shanghai Hitech Instruments Co. Ltd., China).

### Pretreatment of initial MWCNTs and synthesis of the Cu/Cu<sub>x</sub>O@MWCNTs nanocomposites

The initial MWCNTs were purchased from Shenzhen Nanotech Port Co., Ltd., Shenzhen, China. The purification of MWCNTs was approached as reported in our previous study<sup>[35]</sup>. In brief, prior to use, the initial MWCNTs were dispersed in a 3 M solution of nitric acid and treated with the help of ultrasonication for 4 h. Subsequently, the solution was cleaned with deionized water and filtered using a vacuum pump; the MWCNTs slurry collected by filtration was then dried.

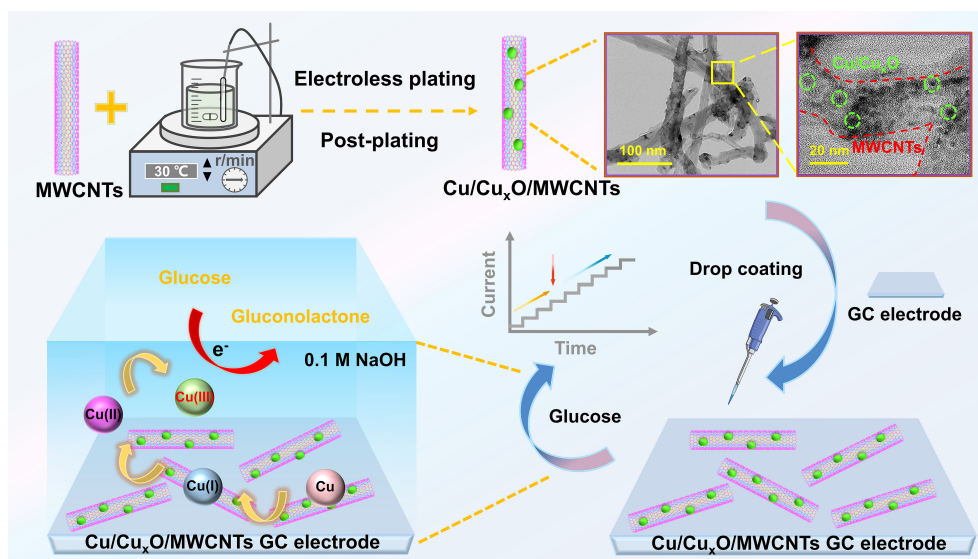
The synthesis of Cu/Cu<sub>x</sub>O@MWCNTs ternary nanocomposites was carried out as follows: sensitization → activation → reduction treatment → plating → post-plating. In order to acquire the homogeneity and integrity of the MWCNTs, the entire process was operated under ultrasonic environment. The formulations and operating conditions regarding to the Cu/Cu<sub>x</sub>O@MWCNTs ternary nanocomposites preparation are displayed in [Table 1](#).

### Characterization

Analyses employing a transmission electron microscope (TEM) and energy dispersive X-ray spectroscopy (EDS) were conducted using the Talos F200X G2 TEM (Thermo Scientific, USA). X-ray diffractometer (XRD) examination was performed by an X'Pert Pro (PANalytical B.V., Netherlands) using Cu Ka

**Table 1. The formulations and operating conditions of synthesizing Cu/Cu<sub>x</sub>O@MWCNTs**

Procedure	Chemicals and operating conditions	Parameters
Sensitization	SnCl <sub>2</sub>	5 g
	T	25 °C
	Time	2-2.5 mins
Activation	PdCl <sub>2</sub>	0.1 g/L
	T	25 °C
	Time	2-2.5 mins
Reduction	NaH <sub>2</sub> PO <sub>2</sub>	15 g/L
Plating	NaOH	7 g/L
	NaK <sub>2</sub> C <sub>4</sub> H <sub>4</sub> O <sub>6</sub> ·4H <sub>2</sub> O	25 g/L
	CuSO <sub>4</sub> ·5H <sub>2</sub> O	5 g/L
	Methanal	12 mL
	T	30 °C
	Time	2-2.5 min
	pH	13-14
Post-plating	Oxidation of Cu	220 °C, 4 h

**Scheme 1.** Schematic diagram of electrochemical sensing using Cu/Cu<sub>x</sub>O@MWCNTs ternary nanocomposites-based sensor.

radiation. X-ray photoelectron spectroscopy (XPS) was analyzed using a Thermofisher Escalab Xi+ (Thermofisher, USA) by Al K $\alpha$  radiation.

### Preparation of the glucose electrochemical sensor and electrochemical measurements

The glassy carbon electrodes (GC, diameters of 3 mm) were used as a substrate for the working electrode fabrication. They were mechanically polished using emery paper, followed by polishing of 0.3 and 0.05  $\mu$ m alumina powder with a polishing cloth, and were alternately ultrasonic bath cleaning for 3 min with pure ethanol and deionized water. Subsequently, these electrodes were modified by dropping 6  $\mu$ L of the Cu/Cu<sub>x</sub>O@MWCNTs ethanol dispersion solution onto the electrode surface and then air-dried. The obtained electrodes were named the Cu/Cu<sub>x</sub>O@MWCNTs-modified GC electrodes.

Additionally, a CHI 660E electrochemical analyzer (Chenhua, Shanghai) was collected to carry out electrochemical experimentations in a two-compartment electrochemical cell at room temperature. In this work, the GC, platinum, and Ag/AgCl electrodes (KCl-saturated) were utilized as the substrates for the fabricated working, counter, and reference electrodes, respectively. For electrochemical impedance spectroscopy (EIS) measurements, the ac voltage was set as 5 mV at an open circuit potential of 0.23 V. The amperometric *i-t* tests were studied by adding various glucose concentrations consecutively at 0.45 V.

## RESULTS AND DISCUSSION

### Characterization of as-synthesized samples

After purification, we observed the morphology of the raw MWCNTs with TEM and characterized their functional groups using Raman spectra. Considering that the surface of MWNT contains residual metal catalytic particles originating from the production process, we subject MWCNTs to acid purification prior to preparing the composites, as previously reported<sup>[35]</sup>. The TEM images and Raman spectra of raw and purified MWCNTs composites are investigated [Figure 1A-C]. Comparing the TEM images exhibited in Figure 1A and B, MWCNTs, before and after purification, exhibit a hollow tubular structure. Additionally, the wall dissolution breakage or damage phenomenon is not detected in MWCNTs following purification. Furthermore, the purification treatment significantly improved the agglomerated degree of initial MWCNTs. In Figure 1A, impurities exist in initial MWCNTs (catalyst metal nanoparticles and amorphous carbons<sup>[36]</sup>). The catalyst metal nanoparticles and amorphous carbon impurities are observed to decrease significantly in Figure 1B. This decrease is mainly attributed to the removal of metal catalyst impurities present in the initial MWCNTs, as they are transformed into metal oxides or hydroxides during the acid purification and thus dissolved in the solution. Meanwhile, since the structural stability of MWCNTs is much greater than that of carbon impurities, the carbon impurities are easier to remove by oxidation in acid solution<sup>[36-38]</sup>. Acid purification not only removes impurities but also introduces oxygen-containing functional groups [Supplementary Figure 1] into the surface defects and tube ends of MWCNTs<sup>[36]</sup>. The impact of these functional groups on MWCNT dispersion in the plating solution and the performance of the modified electrode is significant. Therefore, an acid purification treatment of purchased MWCNTs is both essential and efficient.

Figure 1C records the Raman spectra for MWCNTs. As investigated in Figure 1C, the D-band located near  $1,342\text{ cm}^{-1}$  is mainly derived from the presence of structural defects or disordered structural positions in the MWCNTs associated with the amorphous or disordered carbon. The G-band located near  $1,573\text{ cm}^{-1}$  for initial MWCNTs and  $1,580\text{ cm}^{-1}$  for purified MWCNTs originating from the doubly condensed in-plane optical vibrations of  $\text{sp}^2$  hybridized carbon<sup>[39]</sup>, which is consistent with former studies (G-band at  $\sim 1,580\text{ cm}^{-1}$ <sup>[39,40]</sup>). Generally, the D- to G-band intensity ratio ( $I_D/I_G$ ) is a dependable parameter for evaluating the disorder level in carbon materials<sup>[39]</sup>. In the study, the  $I_D/I_G$  ratio of initial MWCNTs is 1.07, higher than the purified MWCNTs ( $I_D/I_G$  ratio is 1.00), indicating fewer defects or decreased amorphous carbons remaining on the surface of the MWCNTs. It has been shown that nitric acid can effectively eliminate impurities from MWCNTs, leading to higher purity in the MWCNTs. Therefore, the above results further confirm the effectiveness of the acid purified treatment of initial MWCNTs.

The purified MWCNTs were used to prepare Cu/Cu<sub>x</sub>O/MWCNTs ternary nanocomposites, and the morphology and composition characterization was shown in Figure 1D-H. As depicted in Figure 1D and E, the surface of the MWCNTs owns a number of evenly distributed nanoparticles, which increases the specific surface area of the MWCNTs. The increased surface area of the Cu/Cu<sub>x</sub>O@MWCNTs may enhance the direct electron transfer between the Cu/Cu<sub>x</sub>O@MWCNTs and the GC electrode compared with the direct electron transfer between MWCNTs and the bare GC electrode. From the high-resolution

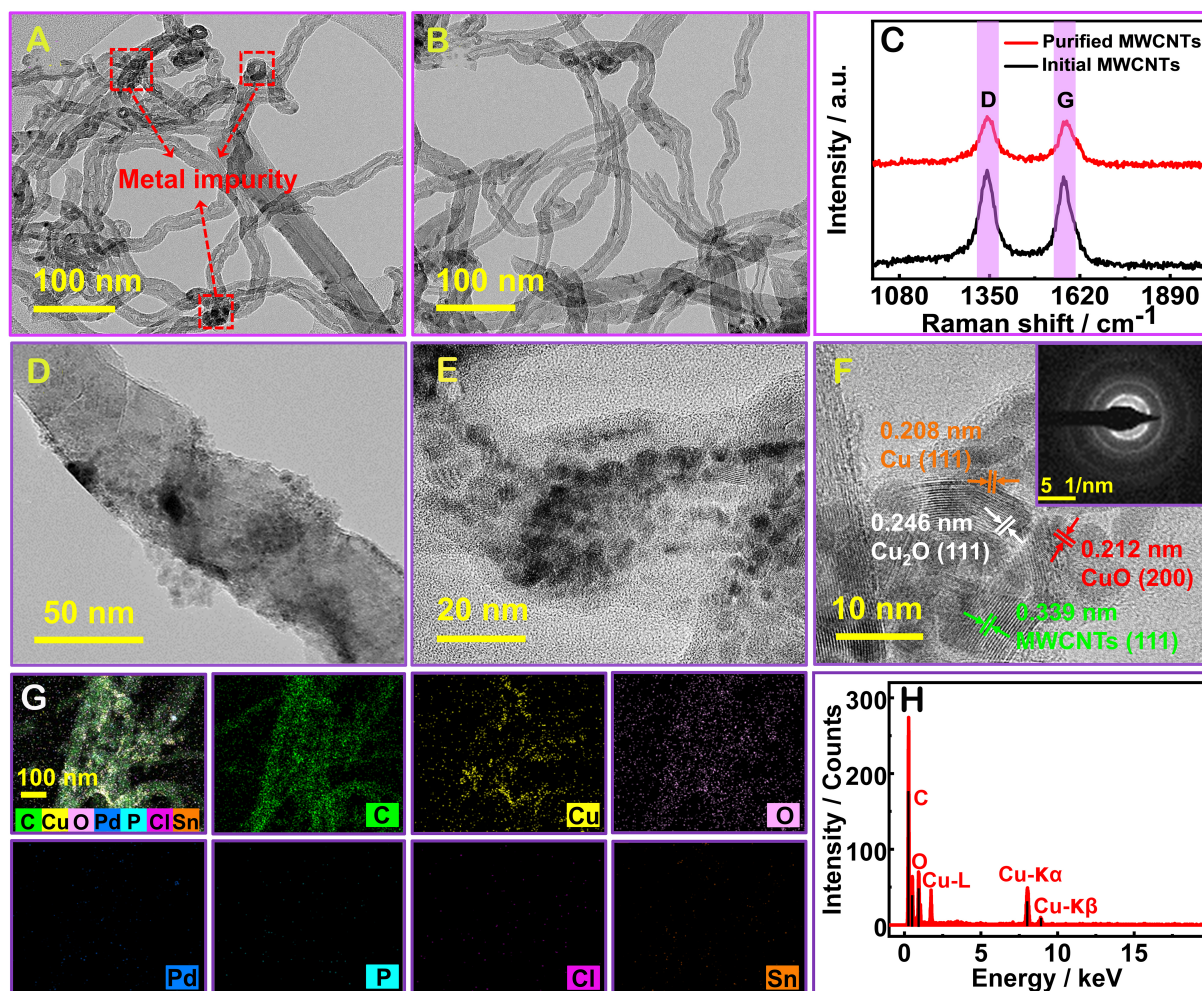


**Figure 1.** (A and B) TEM images of the initial MWCNTs and the purified MWCNTs composites. (C) Raman spectra of the raw MWCNTs and the purified MWCNTs composites at  $\lambda = 532$  nm. (D and E) TEM images of the Cu/Cu<sub>x</sub>O@MWCNTs nanocomposites. (F) HRTEM images of the Cu/Cu<sub>x</sub>O@MWCNTs nanocomposites and the corresponding SAED pattern (insert). (G) TEM-EDX of C, Cu, O, Pd, P, Cl, and Sn elements for the Cu/Cu<sub>x</sub>O@MWCNTs nanocomposites. (H) EDX spectra of the Cu/Cu<sub>x</sub>O@MWCNTs nanocomposites.

transmission electron microscopy (HRTEM) images [Figure 1F], the lattice spacings of these tubular structures are analyzed as 0.339 nm, which is close to the lattice spacing (0.34 nm) of crystal plane (111) of MWCNTs. Herein, the marked lattice spacings of 0.208, 0.246, and 0.212 nm ascribed to the (111) crystal plane of Cu, the (111) crystal plane of Cu<sub>2</sub>O<sup>[15,31]</sup>, and the (200) crystal plane of CuO, respectively. The analysis demonstrates that the as-prepared MWCNTs-based composites are ternary nanocomposites, consisting of Cu, Cu<sub>2</sub>O, and CuO phases. In addition, the corresponding selected area electron diffraction (SAED) pattern (insert for Figure 1F) investigated that the composites exhibit superior polycrystallinity, which is consistent with HRTEM analysis. Figure 1G illustrates the scanning electron microscopy-energy-dispersive X-ray spectrometry (TEM-EDX) elemental mapping of the selected area and the distribution of each component. The analysis reveals that the selected area has a uniform distribution of the elements C, Cu, and O, with no elemental segregation or aggregation. Almost no residue of the impurities, such as Pd, P, Cl, and Sn, may be retained during the electroless plating process. From Figure 1H, the quantitative analysis of the EDS results presents mainly C, O, and Cu elements, confirming the successful construct of the Cu and Cu<sub>x</sub>O onto MWCNTs. Above all, the phase composition of the Cu/Cu<sub>x</sub>O@MWCNTs nanocomposites is fully identified as MWCNTs, Cu, and Cu<sub>x</sub>O. The XRD pattern of the synthesized Cu/Cu<sub>x</sub>O@MWCNTs

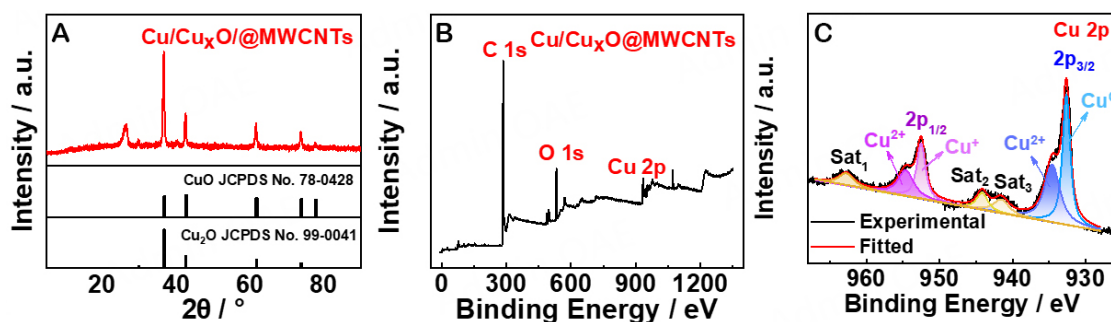


**Figure 2.** (A) XRD patterns of the Cu/Cu<sub>x</sub>O@MWCNTs nanocomposites. The XPS survey scan (B) and the Cu 2p spectrum (C) of the Cu/Cu<sub>x</sub>O@MWCNTs nanocomposites.

[Figure 2A] is exhibited. According to Figure 2A, it is clear that the Cu/Cu<sub>x</sub>O@MWCNTs exhibit a typical characteristic peak at 26.2° via scanning speed of 4°/min attributed to (111) index plane of MWCNTs, which is a valid information for the subsequent research on the integration of ternary nanocomposites with MWCNTs. Then, the sharp characteristic peaks emerge at  $2\theta = 29.6^\circ, 36.4^\circ, 42.3^\circ, 61.4^\circ, 73.5^\circ,$  and  $77.4^\circ$ , which are attributed to (110), (111), (200), (220), (311), and (222) crystal planes of Cu<sub>2</sub>O nanoparticles (JCPDS No. 99-0041), respectively. In addition, the diffraction peaks reflected by the (111) and (200) crystal planes agreeing with CuO nanoparticles (JCPDS No. 78-0428) appear at  $36.6^\circ$  and  $42.5^\circ$ . However, no diffraction peaks are attributed to metal Cu for the nanocomposites, possibly due to the low amount of the metal Cu.

As recorded in Figure 2B and C, the exact composition and valence state of the Cu/Cu<sub>x</sub>O@MWCNTs nanocomposites are further identified through XPS. The high-resolution XPS spectrum of Cu 2p clearly shows Cu 2p<sub>1/2</sub>, 2p<sub>3/2</sub> and satellite peaks. After fitting, the Cu 2p<sub>1/2</sub> peak with 952.5 and 954.6 eV corresponds to Cu<sup>+</sup>[41] and Cu<sup>2+</sup>[42], respectively. The Cu 2p<sub>3/2</sub> peak with 932.6 and 934.6 eV corresponds to Cu<sup>0</sup>[43] and Cu<sup>2+</sup>[44], respectively, proving the existence of Cu<sup>0</sup>, Cu<sup>+</sup> and Cu<sup>2+</sup>, the ratio is 2.43:1.17:3.16 [Supplementary Table 1]. The 941.6, 944.2, and 962.8 eV attribute to satellite peaks[44,45]. These results further indicate the successful synthesis of the MWCNTs-based Cu/Cu<sub>x</sub>O ternary nanocomposites.

### Electrochemical behavior and performance of the electrode

Before developing an electrochemical method for nonenzymatic glucose sensing, it is required to electro-activate the Cu/Cu<sub>x</sub>O@MWCNTs. We process the electrochemical activation by conducting 40-cycle successive cyclic voltammograms (CVs) at a 50 mV·s<sup>-1</sup> scan rate within potential ranging from -0.90 to +0.75 V in alkaline circumstances [Supplementary Figure 2]. All cyclic voltammetry measurements in this paper are performed in N<sub>2</sub>-saturated solutions. The electrochemical behavior of the Cu/Cu<sub>x</sub>O@MWCNTs-based electrodes after electro-activation is investigated by the CV in alkaline solutions (0.1 M NaOH). Figure 3A shows four anodic peaks and three cathodic redox peaks in the potential range -0.90 to +0.75 V. These peaks may be ascribed in a series of consecutively and competitively redox reactions between Cu(0) and copper oxide[46], which governs the electrochemical behavior of the constructed Cu/Cu<sub>x</sub>O@MWCNTs-modified GC electrodes under alkaline supporting electrolyte [Scheme 1]. The emergence of anodic peak 1 could be assigned to the conversion from Cu(0) to Cu(I), at which Cu(0) is transformed to CuOH and Cu<sub>2</sub>O by electrooxidizing. Meanwhile, the anodic peak 2 is attributed to the oxidation of Cu(0) and Cu(I) to Cu(II). There are soluble species derived from Cu(0) and Cu(II) formed at anodic peak 3 and soluble species originating from Cu(II) at peak 4, which is consistent with the findings of previous literature[47]. In the backward scanning direction, the cathodic peaks 5, 6, and 7 accordingly typify the redox of Cu(III) to Cu(II), Cu(II) to Cu(I), and Cu(I) to Cu(0). To sum up, the involving possible mechanism of the

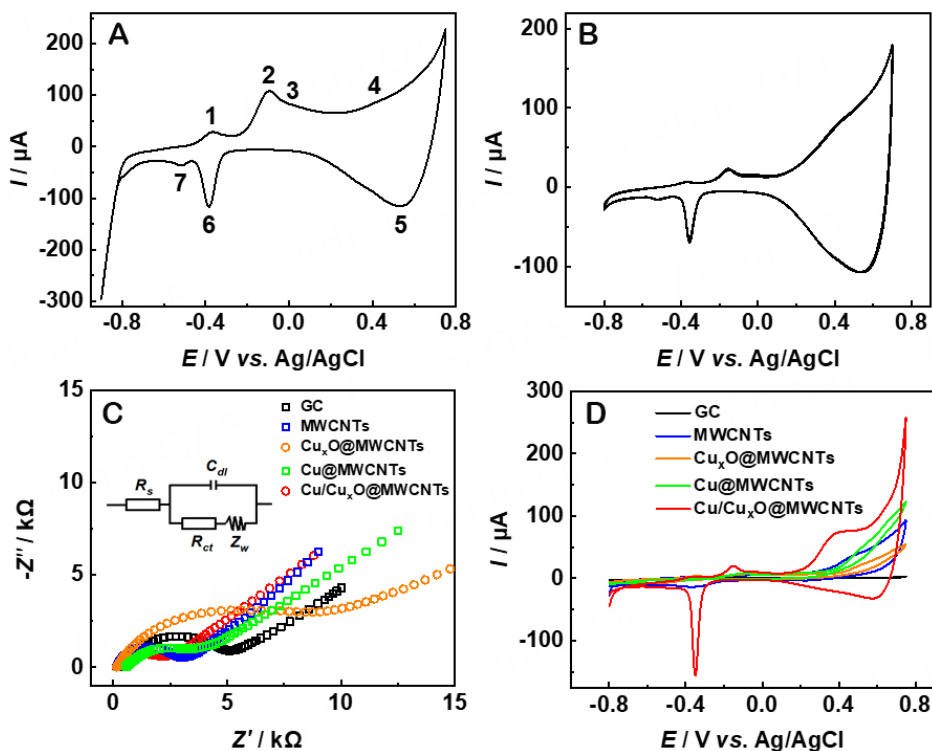


**Figure 3.** (A) The typical cyclic voltammograms of the Cu/Cu<sub>x</sub>O@MWCNTs-modified GC electrode, 0.1 M NaOH, a scanning rate of 50 mV·s<sup>-1</sup>. (B) Successive 50-cycle cyclic voltammograms at Cu/Cu<sub>x</sub>O@MWCNTs-modified GC electrode. (C) Nyquist plots at GC electrode (black curve), MWCNTs-modified GC electrode (blue curve), Cu<sub>x</sub>O@MWCNTs-modified GC electrode (orange curve), Cu/MWCNTs-modified GC electrode (green curve) and Cu/Cu<sub>x</sub>O@MWCNTs-modified GC electrode (red curve) in 0.1 M KCl comprising the 5 mM K<sub>3</sub>[Fe(CN)<sub>6</sub>] solution. Inset: the equivalent circuit. (D) CV curves of GC electrode (black curve), MWCNTs-modified GC electrode (blue curve), Cu<sub>x</sub>O@MWCNTs-modified GC electrode (orange curve), Cu/MWCNTs-modified GC electrode (green curve) and Cu/Cu<sub>x</sub>O@MWCNTs-modified GC electrode (red curve) with 1.0 mM glucose recorded at 20 mV·s<sup>-1</sup>.

electrochemical process could be further explained as follows<sup>[47-50]</sup>:

Peak 1



Peak 2



Peak 3



Peak 4



Peak 5



Peak 6



Peak 7



The above analysis redox results further confirm the successful synthesis of Cu/Cu<sub>x</sub>O@MWCNTs nanocomposites. After accomplishing the electrochemical activation, the constructed Cu/Cu<sub>x</sub>O@MWCNTs-based electrodes are cycled 50 times to examine their electrochemical stability. From [Figure 3B](#), the redox peak currents of the Cu/Cu<sub>x</sub>O@MWCNTs-modified GC electrodes exhibit a decrease by approximately 2.0% after 50 continuous scans, indicating superior stability of the Cu/Cu<sub>x</sub>O ternary nanocomposites integrated with MWCNTs. To study the electron transfer of the electrode/electrolyte interface for the modified electrode during the electrochemical process, we conduct EIS measurements. The semicircle diameters at higher frequencies are equal to the electron transfer resistance ( $R_{ct}$ ), which is inversely proportional to the electron transfer rate constant and indicative of the electron transfer kinetics of the redox probe at the electrode/electrolyte interface. The typical Nyquist plots of the various fabricated electrodes with different nanocomposites in the redox probe of 5 mM K<sub>3</sub>[Fe(CN)<sub>6</sub>] with the frequency of 10<sup>-2</sup> to 10<sup>6</sup> Hz are illustrated in [Figure 3C](#). As shown in [Figure 3C](#), the fitting of the impedance data was performed with the Randles circuit, where  $R_s$ ,  $C_{dl}$ , and  $Z_w$  represent the electrolyte resistance, double layer capacitance, and the Warburg diffusion resistance, respectively. After fabrication with the diverse nanocomposites, the diameter of the semicircle, representing the electron transfer resistance of the modified layer, shifts to show that various materials are attached to the conductive surface of the GC electrode. The order of the  $R_{ct}$  values is Cu/Cu<sub>x</sub>O@MWCNTs < MWCNTs < Cu/MWCNTs < GC < Cu<sub>x</sub>O@MWCNTs-based GC electrodes, with Cu<sub>x</sub>O@MWCNTs-based GC electrodes possessing the highest resistance attributed to the weak electrical conductivity of copper oxides. The resistance to electron transfer of the MWCNTs is lower than GC electrodes, which is particularly explained by high specific surface area and remarkable electrical conductivity of MWCNTs. The analysis results demonstrate that the electron transferring capability of Cu/Cu<sub>x</sub>O@MWCNTs nanocomposites is significantly fast. This proves that

Cu/Cu<sub>x</sub>O@MWCNTs are effectively modified onto the GC surface, facilitating the construction of sensitive nonenzymatic electrochemical sensors.

Herein, to further study this excellent electron transferring capability, cyclic voltammetry is conducted to explore the electrocatalytic activity of the modified electrode towards glucose. As shown in [Figure 3D](#), in the presence of 1.0 mM glucose, glucose oxidation on the GC electrode seems to be very sluggish oxidation with a tailed oxidation, indicating that the glucose electrooxidation on the GC electrode has very low electrochemical kinetics. The oxidation potential of glucose on the MWCNTs-base electrode appears at 0.45 V, possibly owing to the catalytic activity and high specific surface area of the MWCNTs-modified electrode. While, the oxidation potential is 0.46 V on the Cu@MWCNTs-based electrode, lower than the Cu<sub>x</sub>O electrode 0.04 V and higher than the MWCNTs electrode 0.01 V. It is shown that the Cu@MWCNTs material has a weak catalytic effect on glucose with the addition of Cu. As for Cu<sub>x</sub>O@MWCNTs-modified GC electrodes, the high catalytic oxidation potential (0.50 V) may result from the weak catalytic activity of the Cu<sub>x</sub>O material. The oxidation peak is 0.37 V at the Cu/Cu<sub>x</sub>O@MWCNTs-modified GC electrode, exhibiting the lowest oxidation potential compared to the GC, MWCNTs-modified GC, Cu@MWCNTs-modified GC, and Cu<sub>x</sub>O@MWCNTs-modified GC electrodes. This is attributed to large surface area of the Cu/Cu<sub>x</sub>O@MWCNTs materials and the synergies between components in the Cu/Cu<sub>x</sub>O ternary nanocomposites. Herein, MWCNTs serve as support materials to advance the conductivity and increase the specific surface area, facilitating the capture of more glucose onto the electrode surface, while MWCNTs also act as catalysts for glucose. Both copper and copper oxides are known to be catalytic for glucose<sup>[21,31]</sup>; the catalytic efficiency of the ternary composites of Cu/Cu<sub>x</sub>O@MWCNTs is 1.94 and 4.2 folds exceeding that of Cu@MWCNTs and Cu<sub>x</sub>O@MWCNTs, respectively. This indicates that ternary composites have improved catalytic activity over binary and unitary composites. The possible reasons are that higher specific surface area of Cu/Cu<sub>x</sub>O@MWCNTs ternary materials and electrical conductivity of MWCNTs and Cu benefit facilitating the electron transfer. The probable mechanism for glucose electrooxidation on electrodes based on Cu/Cu<sub>x</sub>O@MWCNTs materials is during cyclic voltammetry; Cu, Cu(I) and Cu(II) would be oxidized to Cu(III) based on reactions 1-13 above, which can facilitate the glucose oxidation to produce gluconolactone<sup>[48-50]</sup>. The presence of copper and its oxides promotes the production of Cu(III) so that ternary composites have superior electrocatalytic oxidation properties than binary and unitary composites. The study reveals that the Cu/Cu<sub>x</sub>O@MWCNTs-based electrode shows the highest current response. This is due to the high electron transfer kinetics of the Cu/Cu<sub>x</sub>O@MWCNTs, as supported by the EIS results.

To obtain the kinetics of the electrochemical reaction of glucose at the Cu/Cu<sub>x</sub>O@MWCNTs-modified GC electrode, the CVs of the Cu/Cu<sub>x</sub>O@MWCNTs-modified GC electrodes are further investigated for the influence of scan rate ( $\nu$ ) on the peak currents ( $I_p$ ) in [Figure 4A](#). As the scan rates increase, the glucose oxidation peak current at 0.37 V of the Cu/Cu<sub>x</sub>O@MWCNTs-modified GC electrodes also rises. As shown in [Figure 4B](#), the  $I_p$  is linearly related to  $\nu$ , indicating that the electrochemical process of glucose at Cu/Cu<sub>x</sub>O@MWCNTs-modified electrode is an adsorption-controlled process.

#### Amperometric response of the electrode

We have systemically examined and demonstrated the effective electrocatalytic activity of the Cu/Cu<sub>x</sub>O@MWCNTs enables the efficient electrocatalysis for the glucose electrooxidation. The amperometric response of the Cu/Cu<sub>x</sub>O@MWCNTs nanocomposites to modify GC electrodes for glucose sensing was conducted. Before quantitative analysis, we examine the response of different voltages to glucose for the optimized voltage value suitable for this sensor using amperometric detection. From [Supplementary Figure 3](#), the response to glucose is higher at 0.45 V than at other voltages; therefore, 0.45 V is chosen as the test condition for all of the following tests. [Figure 5A](#) describes the amperometric response of the Cu/Cu<sub>x</sub>O@MWCNTs-modified GC electrode toward continuous addition of glucose into NaOH.

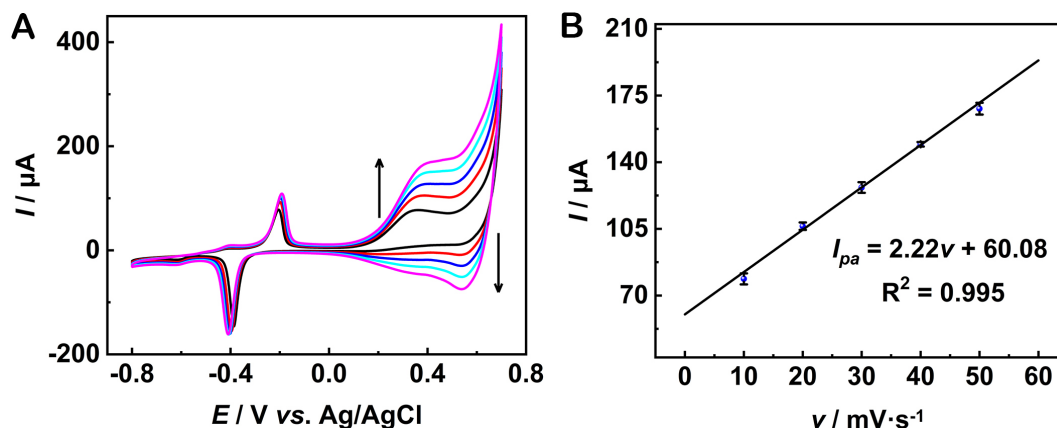


**Figure 4.** (A) Cyclic voltammetry of Cu/Cu<sub>x</sub>O@MWCNTs-modified GC electrode at various scanning rates within various scanning rates with 1.0 mM glucose. The arrows indicate the directions of current rising with increasing scanning rates. (B) The calibration curve,  $n = 3$ .

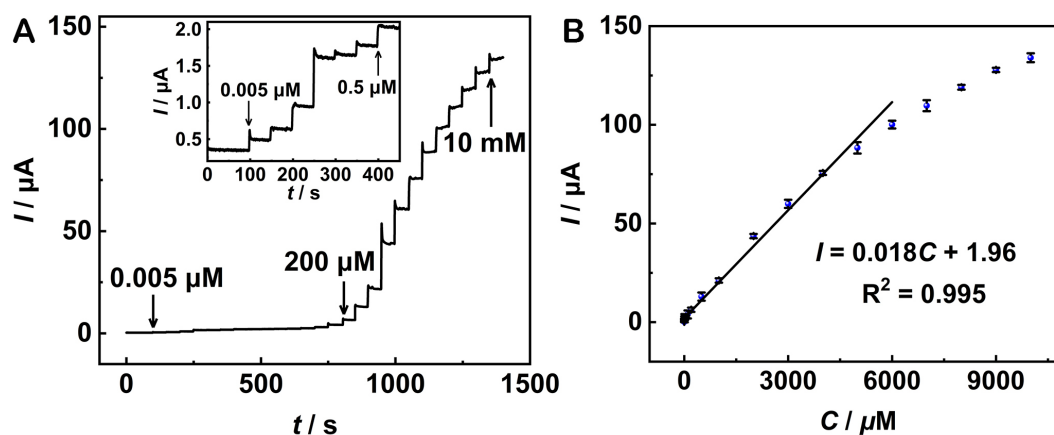


**Figure 5.** (A) Amperometric curve of the response of Cu/Cu<sub>x</sub>O@MWCNTs-modified GC electrode to glucose measured at 0.45 V. The insert is the  $i-t$  curve of the electrode to glucose with consecutive addition of glucose ranging from 0.005 to 0.5  $\mu\text{M}$ . (B) Corresponding calibration plots of  $I$  vs.  $C$ ,  $n = 3$ .

**Figure 5B** records that the current responses of the constructed electrodes are linear with the glucose concentration within a range of 0.005–6,000 M ( $I/\mu\text{A} = 0.018 C/\text{M} + 1.96$ ,  $R^2 = 0.995$ ). The limit of detection (LOD) is calculated to be 0.003  $\mu\text{M}$ , according to the principle of the  $3\sigma/\text{slope}$ , where  $\sigma$  is the standard deviation of a blank signal and the slope is determined from a linear calibration equation at a dynamic concentration range of 0.005–6,000  $\mu\text{M}$ . Additionally, the sensitivity of the Cu/Cu<sub>x</sub>O@MWCNTs-based electrode is 257.14  $\mu\text{A}\cdot\text{mM}^{-1}\cdot\text{cm}^{-2}$ .

**Table 2** compares the results obtained from this work with those of previously reported nonenzymatic glucose sensors. The result reveals that the sensitivity, LOD, and linear detection range are better than those of most reported sensors.

### Selectivity, repeatability, and reproducibility

High selectivity, repeatability, and reproducibility are crucial requirements for practical glucose detection. In blood, glucose usually coexists with small amounts of organic molecules [i.e., dopamine (DA), ascorbic acid (AA), uric acid (UA), 5-Hydroxytryptamine (5-HT) and 3,4-Dihydroxyphenylacetic acid (DOPAC)].

**Table 2. Comparison of the electrochemical performances between Cu/Cu<sub>x</sub>O@MWCNTs-based and other nonenzymatic glucose sensors**

Electrodes	Sensitivity $\mu\text{A}\cdot\text{mM}^{-1}\cdot\text{cm}^{-2}$	Linear range ( $\mu\text{M}$ )	Detection limit ( $\mu\text{M}$ )	Ref.
CuO@MCM-41/Ni foam <sup>a</sup>	0.01723	83-1,500	0.016	[51]
NiO/C@rGO/GCE <sup>b</sup>	-	1-1,115	0.658	[52]
Ni/NiO/NC/GCE <sup>c</sup>	76.03	0.6-8,600	0.2	[53]
ZnO TPs/MXene/GOX <sup>d</sup>	29	50-700	17	[54]
Co-PM-NDGPC/SPE <sup>e</sup>	427.85	30-1,071	7.8	[55]
Pt-MWCNT/SF <sup>f</sup>	8.09	100-3,750	0.1	[56]
GCE/CNT/MoS <sub>2</sub> /NiNPs <sup>g</sup>	-	50-650	0.197	[57]
Cu-BC1/PGE <sup>h</sup>	6214.4	1,000-5,000	0.8	[58]
MoS <sub>2</sub> @CuCo <sub>2</sub> O <sub>4</sub> /GCE <sup>i</sup>	-	0.5-393	0.5	[59]
Cu/Cu <sub>x</sub> O@MWCNTs/GC	257.14	0.005-6,000	0.003	This work

<sup>a</sup>CuO@Mobile crystalline material-41-modified nickel foam electrode; <sup>b</sup>Nickel (gallate) pyrolysis with graphene oxide-modified GC electrode; <sup>c</sup>Ni/NiO/Cellular carbon foam nanocomposite-modified GC electrode; <sup>d</sup>ZnO tetrapods/Ti<sub>3</sub>C<sub>2</sub>T<sub>x</sub> nanoflakes/Glucose oxidase-modified screen printed electrode; <sup>e</sup>Cobalt and polymelamine/nitrogen-doped graphitic porous carbon nanohybrid composite-modified screen-printed electrode; <sup>f</sup>MWCNT/silk fibroin flexible film, decorated with platinum nanoparticles and loaded with glucose oxidase; <sup>g</sup>Carbon nanotubes/MoS<sub>2</sub>/NiNPs-modified GC electrode; <sup>h</sup>Co-deposition of Cu and biochar-modified pencil graphite electrode; <sup>i</sup>MoS<sub>2</sub>@CuCo<sub>2</sub>O<sub>4</sub>-modified GC electrode.

Whereas these organic substances also generate corresponding current signals during the actual detection process, which can influence the glucose detection results. What is more, copper-containing materials-based electrodes are susceptible to chlorine ion poisoning (Cl<sup>-</sup>). Therefore, it is required that the prepared electrode materials must have great anti-interference ability. In order to investigate the interference rejection capability of the Cu/Cu<sub>x</sub>O@MWCNTs-modified electrodes, 10  $\mu\text{M}$  DA, AA, UA, 5-HT, DOPAC, 3 mM Cl<sup>-</sup>, and 500  $\mu\text{M}$  glucose are sequentially added to 0.1 M NaOH solution and repeated three times, as shown in Figure 6A. It is evident from Figure 6A that there is an obvious current response when glucose is added, whereas the current signals obtained from adding small amounts of other interferences are quite weak. Taking the glucose response signal as a benchmark, the response signals of all interferences were converted by percentage, and the results are shown in Figure 6B. Upon analyzing the results, it can be seen that the response signals of the interferences are around 3%, which will not have a dominant effect on the detection results. This further indicates that the as-prepared sensor is resistant to these small amounts of interfering substances mentioned above. Subsequently, we conduct five consecutive amperometric response measurements of 500  $\mu\text{M}$  glucose to assess the repeatability of the Cu/Cu<sub>x</sub>O@MWCNTs-modified GC electrode, resulting in a relative standard deviation (RSD) of 2.1%. Additionally, we tested the reproducibility by comparing the amperometric response of 500  $\mu\text{M}$  glucose using five freshly prepared electrodes [Supplementary Figure 4]. The electrochemical system demonstrates superior reproducibility with an RSD of 1.8% for five separately constructed electrodes.

### Application analysis in serum samples

To assess its analytical utility, the constructed electrochemical sensor is employed for the glucose determination in real samples. Before detection, all of the samples are diluted with 0.1 M NaOH by 50-fold, which can reduce the matrix effect of the serum samples. To evaluate the correctness of the results, a certain amount of glucose is spiked to the sample and the electrochemical results are compared with those of a commercial blood glucose analyzer, yielding consistent results. The results obtained from three samples are studied [Table 3]. The recovery rates of the spiked samples are measured in the range of 100.54% to 102.4% with an RSD of  $5.60 \pm 1.55$  for glucose. This indicates that the developed sensor is both accurate and precise.

**Table 3. Determination results of glucose in human serum samples (n = 3)**

Sample	Concentration of glucose (mM)	Added (mM)	C (mM)	Recovery (%)	Mean RSD (mM)
1	5.0	0.5	5.55	100.5	
2	5.0	0.5	5.55	102.4	5.60 ± 1.55
3	5.1	0.5	5.70	101.8	

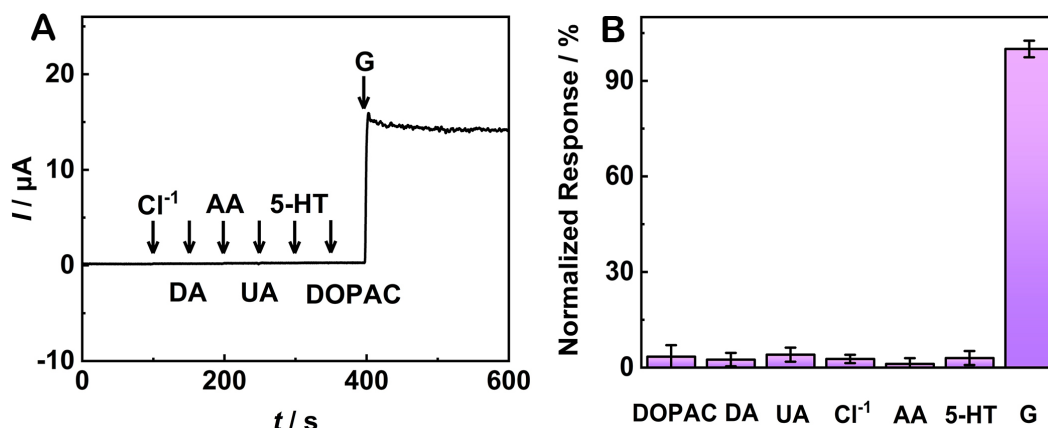


**Figure 6.** (A) The amperometric response of Cu/Cu<sub>x</sub>O@MWCNTs-fabricated GC electrode to the addition of interference species and glucose. (B) The current for Cu/Cu<sub>x</sub>O@MWCNTs-modified GC electrode versus 10 μM DOPAC, 10 μM DA, 10 μM UA, 3 mM Cl<sup>-</sup>, 10 μM AA, 10 μM 5-HT, and 700 μM glucose, n = 3.

## CONCLUSIONS

The Cu/Cu<sub>x</sub>O@MWCNTs ternary nanocomposites were used as an efficient electrocatalyst to construct an electrochemical nonenzymatic sensor toward glucose. The Cu/Cu<sub>x</sub>O@MWCNTs ternary nanocomposites were prepared through the electroless plating process and heat treatment. The Cu/Cu<sub>x</sub>O@MWCNTs-modified GC electrode, based on Cu/Cu<sub>x</sub>O@MWCNTs ternary nanocomposites, exhibited increased current response to glucose, demonstrating rapid response, excellent linearity, and superior sensitivity, repeatability and reproducibility. The nonenzymatic electrochemical sensor demonstrated high selectivity and sensitivity for glucose detection in human serum samples.

## DECLARATIONS

### Authors' contributions

Conceptualization, investigation, methodology, data curation, formal analysis, writing - original draft: Xi W

Investigation, validation, supervision: Zhang Y

Writing - original draft: Zhang Z

Validation, supervision: Chen Y

Writing - review & editing, Formal analysis: Huang X

Methodology, formal analysis: Mou H, Deng Z

Conceptualization, supervision, writing - review & editing: Li Z

Investigation, methodology, writing - review & editing, supervision: Xu X

Formal analysis, supervision, project administration, writing - review & editing, resources: Zheng W

**Availability of data and materials**

Not applicable.

**Financial support and sponsorship**

None.

**Conflicts of interest**

All authors declared that there are no conflicts of interest.

**Ethical approval and consent to participate**

Not applicable.

**Consent for publication**

Not applicable.

**Copyright**

© The Author(s) 2024.

**REFERENCES**

1. Golsanamlou Z, Mahmoudpour M, Soleymani J, Jouyban A. Applications of advanced materials for non-enzymatic glucose monitoring: from invasive to the wearable device. *Crit Rev Anal Chem* 2023;53:1116-31. DOI
2. Cho NH, Shaw JE, Karuranga S, et al. IDF diabetes Atlas: global estimates of diabetes prevalence for 2017 and projections for 2045. *Diabetes Res Clin Pract* 2018;138:271-81. DOI
3. Shen L, Liang Z, Chen Z, et al. Reusable electrochemical non-enzymatic glucose sensors based on Au-inlaid nanocages. *Nano Res* 2022;15:6490-9. DOI
4. Bollella P. Enzyme-based amperometric biosensors: 60 years later ... Quo Vadis? *Anal Chim Acta* 2022;1234:340517. DOI
5. Clark LC Jr, Lyons C. Electrode systems for continuous monitoring in cardiovascular surgery. *Ann N Y Acad Sci* 1962;102:29-45. DOI PubMed
6. Updike SJ, Hicks GP. The enzyme electrode. *Nature* 1967;214:986-8. DOI PubMed
7. Karyakin AA. Glucose biosensors for clinical and personal use. *Electrochem Commun* 2021;125:106973. DOI
8. Vashist SK. Non-invasive glucose monitoring technology in diabetes management: a review. *Anal Chim Acta* 2012;750:16-27. DOI PubMed
9. Sun Y, Shu T, Ma J, et al. Rational design of ZIF-8 for constructing luminescent biosensors with glucose oxidase and AIE-type gold nanoclusters. *Anal Chem* 2022;94:3408-17. DOI
10. Kucherenko IS, Soldatkin OO, Kucherenko DY, Soldatkina OV, Dzyadevych SV. Advances in nanomaterial application in enzyme-based electrochemical biosensors: a review. *Nanoscale Adv* 2019;1:4560-77. DOI PubMed PMC
11. Du Y, Zhang X, Liu P, Yu DG, Ge R. Electrospun nanofiber-based glucose sensors for glucose detection. *Front Chem* 2022;10:944428. DOI PubMed PMC
12. Morshed J, Nakagawa R, Hossain MM, Nishina Y, Tsujimura S. Disposable electrochemical glucose sensor based on water-soluble quinone-based mediators with flavin adenine dinucleotide-dependent glucose dehydrogenase. *Biosens Bioelectron* 2021;189:113357. DOI PubMed
13. Tutel Y, Koylan S, Tunca S, Unalan HE. Nanometer-thick Mn:NiO and Co:NiO films for high performance nonenzymatic biosensors. *ACS Appl Nano Mater* 2021;4:13871-83. DOI
14. Chao D, Chen J, Dong Q, Wu W, Qi D, Dong S. Ultrastable and ultrasensitive pH-switchable carbon dots with high quantum yield for water quality identification, glucose detection, and two starch-based solid-state fluorescence materials. *Nano Res* 2020;13:3012-8. DOI
15. Feng T, Yu C, Manaye Kabtamu D, Bu L, Li F, Wang Y. Cu<sub>2</sub>O nanowires with exposed {111} facet for nonenzymatic detection of glucose in complex biological fluids. *Chem Eng J* 2022;429:132267. DOI
16. Zhou Y, Hu Q, Yu F, et al. A metal-organic framework based on a nickel bis(dithiolene) connector: synthesis, crystal structure, and application as an electrochemical glucose sensor. *J Am Chem Soc* 2020;142:20313-7. DOI
17. Cohen R, Cohen Y, Mukha D, Yehezkeili O. Oxygen insensitive amperometric glucose biosensor based on FAD dependent glucose dehydrogenase co-entrapped with DCPIP or DCNQ in a polydopamine layer. *Electrochim Acta* 2021;367:137477. DOI
18. Dong L, Ren S, Zhang X, Yang Y, Wu Q, Lei T. In-situ synthesis of Pt nanoparticles/reduced graphene oxide/cellulose nanohybrid for nonenzymatic glucose sensing. *Carbohydr Polym* 2023;303:120463. DOI
19. Ghanam A, Haddour N, Mohammadi H, Amine A, Sabac A, Buret F. A membrane-less glucose/O<sub>2</sub> non-enzymatic fuel cell based on

- bimetallic Pd-Au nanostructure anode and air-breathing cathode: towards micro-power applications at neutral pH. *Biosens Bioelectron* 2022;210:114335. DOI
20. Wang Y, Kong J, Xue R, et al. Highly stable, stretchable, and transparent electrodes based on dual-headed Ag@Au core-sheath nanomatchsticks for non-enzymatic glucose biosensor. *Nano Res* 2023;16:1558-67. DOI
  21. Edet HO, Louis H, Godwin UC, Adaliku SA, Agwamba EC, Adeyinka AS. Single-metal (Cu, Ag, Au) encapsulated gallium nitride nanotube (GaNNT) as glucose nonenzymatic nanosensors for monitoring diabetes: perspective from DFT, visual study, and MD simulation. *J Mol Liq* 2023;384:122209. DOI
  22. Dai Z, Yang A, Bao X, Yang R. Facile non-enzymatic electrochemical sensing for glucose based on Cu<sub>2</sub>O-BSA nanoparticles modified GCE. *Sensors* 2019;19:2824. DOI PubMed PMC
  23. Chen J, Liu G, Xiao Q, et al. Glucose biosensors based on pinecone-shaped Au and Ni nanoparticle composite microelectrodes. *ACS Appl Nano Mater* 2022;5:13319-31. DOI
  24. Meng A, Hong X, Zhang Y, et al. A free-standing flexible sensor MnO<sub>2</sub>-Co/rGO-CNT for effective electrochemical hydrogen peroxide sensing and real-time cancer biomarker assaying. *Ceram Int* 2023;49:2440-50. DOI
  25. Hussain MH, Fook LP, Sanira Putri MK, Tan HL, Abu Bakar NF, Radacs N. Advances on ultra-sensitive electrospun nanostructured electrochemical and colorimetric sensors for diabetes mellitus detection. *Nano Mater Sci* 2021;3:321-43. DOI
  26. Alanazi N, Selvi Gopal T, Muthuramamoorthy M, et al. Cu<sub>2</sub>O/MXene/rGO ternary nanocomposites as sensing electrodes for nonenzymatic glucose sensors. *ACS Appl Nano Mater* 2023;6:12271-81. DOI
  27. Yang M, Jeong JM, Lee KG, Kim DH, Lee SJ, Choi BG. Hierarchical porous microspheres of the Co<sub>3</sub>O<sub>4</sub>@graphene with enhanced electrocatalytic performance for electrochemical biosensors. *Biosens Bioelectron* 2017;89:612-9. DOI
  28. Chavez-Urbiola IR, Reséndiz-Jaramillo AY, Willars-Rodriguez FJ, et al. Glucose biosensor based on a flexible Au/ZnO film to enhance the glucose oxidase catalytic response. *J Electroanal Chem* 2022;926:116941. DOI
  29. Zhang X, Wang L, Ji R, Yu L, Wang G. Nonenzymatic glucose sensor based on Cu-Cu<sub>2</sub>S nanocomposite electrode. *Electrochem Commun* 2012;24:53-6. DOI
  30. Yang Y, Li P, Zheng X, et al. Anion-exchange membrane water electrolyzers and fuel cells. *Chem Soc Rev* 2022;51:9620-93. DOI
  31. Yu Z, Wu H, Xu Z, Yang Z, Lv J, Kong C. Wearable noninvasive glucose sensor based on Cu<sub>x</sub>O NFs/Cu NPs Nanocomposites. *Sensors* 2023;23:695. DOI PubMed PMC
  32. Fan L, Wu R, Patel V, Huang JJ, Selvaganapathy PR. Solid-state, reagent-free and one-step laser-induced synthesis of graphene-supported metal nanocomposites from metal leaves and application to glucose sensing. *Anal Chim Acta* 2023;1264:341248. DOI PubMed
  33. Sudharsan S, Rajaram R, Kumar S, Swaminathan P, Ramanujam K, Neelakantan L. Copper oxide anchored polyaniline modified glassy carbon electrode: a new sensor platform for the amperometric determination of chlorpyrifos. *Electrochim Acta* 2023;471:143305. DOI
  34. Zhu T, Zhang Y, Luo L, Zhao X. Facile fabrication of NiO-decorated double-layer single-walled carbon nanotube buckypaper for glucose detection. *ACS Appl Mater Interfaces* 2019;11:10856-61. DOI PubMed
  35. Deng Z, Zhao L, Mu H, et al. High selective property of gelatin/MWCNTs functionalized carbon fiber microelectrode: toward real-time monitoring of ascorbate. *J Electroanal Chem* 2022;914:116315. DOI
  36. Zhang XX, Deng CF, Xu R, Wang DZ. Oxidation resistance of multi-walled carbon nanotubes purified with sulfuric and nitric acids. *J Mater Sci* 2007;42:8377-80. DOI
  37. Hsu HL, Jehng JM, Sung Y, Wang LC, Yang SR. The synthesis, characterization of oxidized multi-walled carbon nanotubes, and application to surface acoustic wave quartz crystal gas sensor. *Mater Chem Phys* 2008;109:148-55. DOI
  38. Liu CK, Wu JM, Shih HC. Application of plasma modified multi-wall carbon nanotubes to ethanol vapor detection. *Sens Actuat B Chem* 2010;150:641-8. DOI
  39. Hu X, Zuo S, Yang M. High-yield preparation of ultrahigh-hydrophilicity MWCNTs by highly controllable oxidation with concentrated HNO<sub>3</sub>/HClO<sub>4</sub> mixture. *Appl Surf Sci* 2023;626:157200. DOI
  40. Liu X, Wang C, Huang Z, Zhu P. Electrospun multiwall nanotubes-loaded polyethylene glycol/polyacrylonitrile composite form-stable nanofibers for thermal energy storage. *J Energy Stor* 2023;66:107458. DOI
  41. Jolley JG, Geesey GG, Hankins MR, Wright RB, Wichlacz PL. Auger electron and X-ray photoelectron spectroscopic study of the biocorrosion of copper by alginic acid polysaccharide. *Appl Surf Sci* 1989;37:469-80. DOI
  42. Jiang J, Liu XX, Han J, Hu K, Chen JS. Self-supported sheets-on-wire CuO@Ni(OH)<sub>2</sub>/Zn(OH)<sub>2</sub> nanoarrays for high-performance flexible quasi-solid-state supercapacitor. *Processes* 2021;9:680. DOI
  43. Santra AK, Rao CNR. Surface alloy formation in Pd/Ag, Cu/Au and Ni/Au bimetallic overlayers. *Appl Surf Sci* 1995;84:347-50. DOI
  44. Parmigiani F, Sangaletti L. The Cu<sub>2p</sub> X-ray photoelectron core-lines in copper oxide based high temperature superconductors. *J Electron Spectrosc Relat Phenom* 1994;66:223-39. DOI
  45. Liu S, Hui KS, Hui KN. Flower-like copper cobaltite nanosheets on graphite paper as high-performance supercapacitor electrodes and enzymeless glucose sensors. *ACS Appl Mater Interfaces* 2016;8:3258-67. DOI
  46. Le WZ, Liu YQ. Preparation of nano-copper oxide modified glassy carbon electrode by a novel film plating/potential cycling method and its characterization. *Sens Actuat B Chem* 2009;141:147-53. DOI
  47. Paixão TRLC, Corbo D, Bertotti M. Amperometric determination of ethanol in beverages at copper electrodes in alkaline medium. *Anal Chim Acta* 2002;472:123-31. DOI

48. Hou L, Zhao H, Bi S, Xu Y, Lu Y. Ultrasensitive and highly selective sandpaper-supported copper framework for non-enzymatic glucose sensor. *Electrochim Acta* 2017;248:281-91. DOI
49. Marioli JM, Kuwana T. Electrochemical characterization of carbohydrate oxidation at copper electrodes. *Electrochim Acta* 1992;37:1187-97. DOI
50. Zhang Y, Su L, Manuzzi D, et al. Ultrasensitive and selective non-enzymatic glucose detection using copper nanowires. *Biosens Bioelectron* 2012;31:426-32. DOI
51. Zohaa, Arif D, Hassan M, et al. An electrochemical sensor based on copper oxide nanoparticles loaded on a mesoporous MCM-41 for non-enzymatic detection of glucose. *Ceram Int* 2024;50:12614-20. DOI
52. Imanzadeh H, Amiri M, Nozari-Asbemarz M. A novel NiO/C@rGO nanocomposite derived from Ni(gallate): a non-enzymatic electrochemical glucose sensor. *Microchem J* 2024;199:110106. DOI
53. Liang H, Luo Y, Xiao Y, Chen R, Wang L, Song Y. Ni/NiO/carbon derived from covalent organic frameworks for enzymatic-free electrochemical glucose sensor. *Ceram Int* 2024;50:977-84. DOI
54. Myndrul V, Coy E, Babayevska N, et al. MXene nanoflakes decorating ZnO tetrapods for enhanced performance of skin-attachable stretchable enzymatic electrochemical glucose sensor. *Biosens Bioelectron* 2022;207:114141. DOI
55. Elanchezian M, Prakasham K, Eswaran M, et al. Eco-friendly fabrication of nonenzymatic electrochemical sensor based on cobalt/polymelamine/nitrogen-doped graphitic-porous carbon nanohybrid material for glucose monitoring in human blood. *Environ Res* 2023;223:115403. DOI
56. Kuang D, Yu W, Liu J, Yin Y, Wang C. Flexible MWCNT/silk fibroin film decorated with Pt NPs for electrochemical glucose sensors. *Microchem J* 2023;191:108760. DOI
57. Fall B, Sall DD, Hémadi M, et al. Highly efficient non-enzymatic electrochemical glucose sensor based on carbon nanotubes functionalized by molybdenum disulfide and decorated with nickel nanoparticles (GCE/CNT/MoS<sub>2</sub>/NiNPs). *Sens Actuat Rep* 2023;5:100136. DOI
58. Larasati LD, Ateş A, Oskay KO. Direct co-deposition of binder-free Cu-biochar-based nonenzymatic disposable sensing element for electrochemical glucose detection. *Surf Interfaces* 2023;42:103355. DOI
59. Wang H, Zhu W, Xu T, et al. An integrated nanoflower-like MoS<sub>2</sub>@CuCo<sub>2</sub>O<sub>4</sub> heterostructure for boosting electrochemical glucose sensing in beverage. *Food Chem* 2022;396:133630. DOI